231 (2023) 212255

Contents lists available at ScienceDirect

Geoenergy Science and Engineering

journal homepage: www.sciencedirect.com/journal/geoenergy-science-and-engineering

Evaluation of distributed damping subs with active control for stick–slip reduction in drilling

Pauline Marie Nüsse [a,*], Adrian Ambrus [b], Ulf Jakob Flø Aarsnes [c], Ole Morten Aamo [a]

[a] Department of Engineering Cybernetics, Norwegian University of Science and Technology, Trondheim, Norway
[b] NORCE Norwegian Research Centre, Stavanger, Norway
[c] NORCE Norwegian Research Centre, Oslo, Norway

ARTICLE INFO

Keywords:
Damping sub
Vibration mitigation
Stick–slip vibration
Active control

ABSTRACT

Drill string vibrations can cause damage to the equipment and reduce drilling performance. There are two primary methods to address this issue: top drive control or the use of specialized tools near the bottom hole assembly (BHA). Another previously published idea is to have several torsional damping sleeves along the drill string, adding viscous damping to the system. The sleeves are designed to be non-rotating, held in place by static friction, but if the combination of braking coefficient and relative pipe velocity gets too high, the sleeve will slip. This paper examines the effectiveness of active control of the braking coefficient, using an On–Off-based control scheme with proportional control. Stability maps are employed to assess the effects of this control scheme on the system for various combinations of top drive feed rates and revolutions per minute (RPM) set points. Such maps allow for a performance comparison of passive sleeves and active sleeves. The results show that active control can improve the drill string behavior both when drilling and when rotating off-bottom, by reducing the slippage of the sleeves. The settling time is reduced to up to a third of the settling time of the passive sleeves.

1. Introduction

To reach and exploit subsurface oil and gas reservoirs or geothermal energy, drilling wells is indispensable. Reaching several kilometers deep, their slenderness ratio makes drill strings prone to vibrations, which can be divided into axial, torsional, and lateral vibrations, regarding in which direction the vibrations are effective. One of the most severe forms of torsional vibrations is stick–slip (Ghasemloonia et al., 2015), mainly caused by the mechanical friction between the drill string and the borehole or casing wall. When the drill pipe is resting along the borehole wall, and a rotation is applied to the pipe, first the static friction will counteract this movement and the pipe stays stationary. The pipe will accumulate the torque until the break-off torque is reached and the pipe suddenly starts moving, releasing the accumulated energy. Since the kinetic friction is lower than the static friction, this leads to peak velocities much higher than the set point. The angular energy is reflected at the top drive forcing the pipe back to a standstill, starting a new stick–slip cycle, unless sufficient energy is dissipated (Aarsnes and Shor, 2018). Such vibrations can harm the drill string in two ways: If the frequency of the vibration is close to the natural frequency of the drill string it can cause a resonance which can lead to breaking failure of the tool. However, more often the vibrations are present for multiple cycles, leading to increased wear, tool fatigue, and reduced drilling performance (Dong and Chen, 2016). Tool failure in any case leads to longer downtime, increased costs, and reduced efficiency.

1.1. State of the art

The mitigation of drilling vibrations receives significant research interest. Two main approaches have been proposed: Either via active control of the top drive or by using special downhole tools. The top drive control entails replacing the industry standard high gain PI controller with newer control schemes such as SoftTorque or ZTorque (Dwars, 2015), which tries to reduce the amount of angular energy reflected at the top drive over a certain frequency range (Aarsnes et al., 2018). Another approach is to use an angular startup velocity trajectory of the top drive to avoid initiating the stick–slip when the drill string overcomes the static friction (Aarsnes et al., 2018). In the literature also other controllers are tested, e.g. based on dynamic programming to find an optimal control strategy (Feng et al., 2017).

* Corresponding author.
E-mail addresses: pauline.nusse@ntnu.no (P.M. Nüsse), aamb@norceresearch.no (A. Ambrus), ulaa@norceresearch.no (U.J.F. Aarsnes), ole.morten.aamo@ntnu.no (O.M. Aamo).

https://doi.org/10.1016/j.geoen.2023.212255
Received 24 May 2023; Received in revised form 3 August 2023; Accepted 14 August 2023
Available online 19 August 2023

The main disadvantages of top drive control are that its effect on the bit movement is limited in long and deviated wells and that it interferes with the tracking control objective of maintaining the RPM set point.

That is where the second approach comes in, placing vibration-damping subs close to the BHA. Various concepts are found here as well, which can be divided into passive or active dampers. While passive dampers have the same configuration while downhole, the characteristics of active tools change while drilling to react to the occurring vibrations. The anti-stall tool (Wildemans et al., 2019) is such a passive device that consists of an axial spring and a helical spline. A torsional load screws the tool together, reducing the axial and torsional load on the bit. The mechanical design of the passive device presented in Kulke et al. (2021) has a torsional friction damper. This damper is limited in range, forcing a shock when the displacement gets too big. A mitigation tool for high-frequency torsional oscillation was built into a rotary steerable system in Wilson et al. (2022). The energy of the oscillations is transferred to an inertia ring via a viscous fluid. In Barton et al. (2011) and Azike-Akubue et al. (2012) the drilling agitator tool or axial oscillation tool is presented; it actively forces small axial vibrations to reduce the mechanical friction and allows a better weight transfer to the bit. Another approach is a shock sub combined with magnetorheological (MR) fluid. The characteristics of the MR fluid can be changed by applying a magnetic field. This changes the viscous damping within the system (Hutchinson, 2013). More MR dampers are investigated in Zhao (2020).

A more recent idea is to use several damping subs distributed along the drill string to meet the distributed nature of sources of excitation of drill string vibrations. A passive version of such subs was presented in Ambrus et al. (2022). Non-rotating sleeves with spur wheels are used to decouple the axial and torsional friction forces. In Holsaeter et al. (2023) a lab setup is shown to verify the functionality of such sleeves experimentally. Here, a PID controller is used for the active control of one sleeve, which is not able to slip due to the constraints of the experimental setup. The design principles behind this sleeve are presented in Cayeux and Ambrus (2023). Here one sleeve per stand is used. The main purpose of the sleeve is to decrease the mechanical friction to reduce the required top drive torque while inducing viscous damping to mitigate vibrations. The sleeves surround the drill pipe. While the sleeve is meant to be non-rotating, the pipe can rotate freely inside the sleeve as it is supported on thrust bearings. Having several such sleeves with larger diameter along the drill string lifts the latter up from the borehole wall. This reduces the mechanical friction affecting the drill pipe as it is mainly focused on the sleeves. These are equipped with spur wheels to reduce friction in the axial direction. Instead of MR fluid, as used in the damping tools reviewed above, the sleeves employ an eddy current brake to induce viscous damping. Briefly explained, a magnet array is placed within the sleeve, while a conductive non-magnetic counterpart is fixed on the drill pipe. The braking force depends on the relative angular velocity between the sleeve and the pipe and on the area of the conductive material exposed to the magnetic field. To allow for active control, the magnet array is movable so the part of the conductive material exposed to the magnetic field can be changed. To have a higher effect, the conductive part can be crenelated, as with decreasing thickness of the material, the resulting braking coefficient decreases (Cayeux and Ambrus, 2023).

1.2. Scope of the paper

This paper investigates what effect active control can have on the damping characteristics of the aforementioned sleeves, using simulations done with a hybrid drill string model. Having one sleeve per stand as in Cayeux and Ambrus (2023) may not be practical due to costs and operational limitations. While fewer sleeves require larger damping coefficients to be effective at vibration mitigation than in the case with many sleeves, active control can help improve the performance when only a few sleeves are used. While drilling, the location of the sleeve in the well changes, and thereby the normal force on the sleeves and consequently the maximum braking force that can be applied changes as well. This means that the braking force of the sleeves has to be changed depending on location, however, communication with the sleeves is not possible. Thus a control has to be based only on local measurements. Compared to Cayeux and Ambrus (2023) only six sleeves are used, whereas instead of passive damping such as in Ambrus et al. (2022) active control is used. In contrast to Holsaeter et al. (2023) the sleeve can slip, requiring the controller to handle such situations.

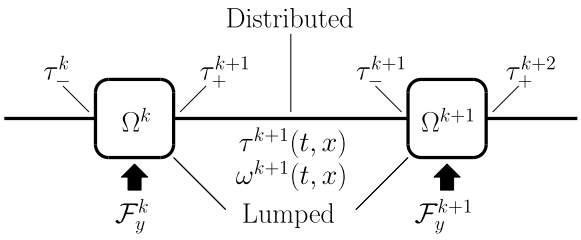

Fig. 1. Hybrid model exemplary for torsional dynamics.
Source: Adapted from Ambrus et al. (2022).

The paper is organized as follows. In Section 2 the hybrid model of the drill string from Ambrus et al. (2022) is revisited and extended to an active sleeve. Section 3 presents the used controllers, with which the simulation results in Section 4 are produced. In Section 5 the effectiveness of passive and active sleeves is investigated for a larger range of feed rate and top drive RPM, followed by conclusions in Section 6.

2. Model

The model used in this paper extends the one presented in Ambrus et al. (2022). The drill string there is modeled as a hybrid between wave equations and lumped elements. In this approach, the drill string is split into N lumped elements with a wave model connecting the lumped elements. A snippet of this hybrid model is sketched in Fig. 1. The lumped elements model, among others, the contact between the borehole and the drill pipe, while the wave equations part models the propagation of axial and torsional waves across the drill-string length. The distributed model in section k is given as

$$\frac{\partial w^k(t,x)}{\partial t} + AE\frac{\partial v^k(t,x)}{\partial x} = 0 \tag{1}$$

$$A\rho\frac{\partial v^k(t,x)}{\partial t} + \frac{\partial w^k(t,x)}{\partial x} = 0 \tag{2}$$

$$\frac{\partial \tau^k(t,x)}{\partial t} + JG\frac{\partial \omega^k(t,x)}{\partial x} = 0 \tag{3}$$

$$J\rho\frac{\partial \omega^k(t,x)}{\partial t} + \frac{\partial \tau^k(t,x)}{\partial x} = 0 \tag{4}$$

where A is the cross-section area, E the elastic modulus, J the polar moment of inertia, G the shear modulus and ρ the density of the pipe. The axial velocity $v(t,x)$ and force $w(t,x)$ as well as the angular velocity $\omega(t,x)$ and torque $\tau(t,x)$ are functions on $\{(t,x)|0 < t < T, x \in [0,l]\}$ with T being some positive time and l the length of the distributed section. The wave equation is simulated using Riemann invariants and an upwind scheme, see Ambrus et al. (2022) for details.

The dynamics of the drill string in the lumped element $k \in [1,\dots,N]$ is given by

$$\dot{V}^k M^k = w_-^k - w_+^{k+1} - \mathcal{F}_x^k - c_a V^k \tag{5}$$

$$\dot{\Omega}^k I^k = \tau_-^k - \tau_+^{k+1} - r_o^k \mathcal{F}_y^k - c_t \Omega^k \tag{6}$$

where V^k and Ω^k are the axial and rotational velocities of the lumped element, respectively. w_-^k and τ_-^k are the axial and torsional forces acting on the element from the pipe above and w_+^{k+1} and τ_+^{k+1} are the

axial and torsional forces acting on the element from the pipe below, that is

$$w_-^k := w^k(t,l) \tag{7}$$

$$\tau_-^k := \tau^k(t,l) \tag{8}$$

$$w_+^{k+1} := w^{k+1}(t,0) \tag{9}$$

$$\tau_+^{k+1} := \tau^{k+1}(t,0)\,. \tag{10}$$

M^k and I^k are the mass and moment of inertia of the lumped element. The outer radius of the drill pipe is r_o^k and the structural damping coefficient in axial and torsional direction are depicted by c_a and c_t. The friction forces between the borehole and the drill pipe in axial and torsional direction are given by $\mathcal{F}_x^k$ and $\mathcal{F}_y^k$, respectively. They are modeled as a Coulomb friction force $\vec{\mathcal{F}}_c = \langle \mathcal{F}_x\, \mathcal{F}_y \rangle$ given by

$$\begin{cases} \vec{\mathcal{F}}_c \in \mathbb{R}^2 : \lfloor \vec{\mathcal{F}}_c \rfloor \in [0,\, \mu_s F_N], & |\vec{v}| < v_c \\ \vec{\mathcal{F}}_c = \mu_k F_N \frac{\vec{v}}{|\vec{v}|}, & |\vec{v}| \geq v_c \end{cases} \tag{11}$$

where $\vec{v} = \langle V\, r_o\Omega \rangle$, v_c is the transition velocity from static to kinetic friction, and μ_s and μ_k are the respective friction coefficients. The side force at the borehole wall is F_N.

The top drive torque, τ_m, and a constant axial feed, V_0, define the upper boundary. The top drive torque is controlled by a PI controller to assure the set point velocity Ω_0 at the top drive. The lower boundary is either defined by the bit–rock interaction (on-bottom case) or set to zero (off-bottom case). In the on-bottom case, the boundaries are $w_+^{N+1} = w_b$, $\tau_+^{N+1} = \tau_b$ where w_b, τ_b are the weight on bit and torque on bit. These are decomposed into cutting and frictional components, indicated by w_c and w_f, respectively, for the weight on bit, and τ_c and τ_f for the torque on bit. The cutting and friction terms are expressed as a function of the bit and rock properties, according to the Detournay bit-rock model for polycrystalline diamond compact (PDC) bits (Detournay et al., 2008)

$$w_b = w_c + g_a(V_b) w_f = \left[\zeta \varepsilon d + g_a(V_b) w_f^*\right] r_b \tag{12}$$

$$\tau_b = \tau_c + g_a(V_b) \tau_f = \left[\varepsilon d + g_a(V_b) \mu \gamma w_f^*\right] \frac{r_b^2}{2} \tag{13}$$

with the bit axial velocity V_b, the ratio of vertical and horizontal forces acting on the PDC cutter face ζ, the intrinsic specific energy of the rock ε, the depth of cut per revolution d, the force per unit length on the wear flat w_f^* (assumed to be constant here), the bit radius r_b, the sliding friction coefficient μ and a bit geometry parameter γ. The function $g_a(V_b)$ adjusts Eqs. (12) and (13) for the case when V_b changes sign or becomes zero in the case of a stuck bit (see Ambrus et al. (2022) for details).

If sleeves are utilized, let $S \subset [1, \ldots, N]$ define the set of indices at which the sleeves are mounted. A sleeve replaces the torsional friction force in the pipe segment $k \in S$ with its braking force F_S

$$F_S^k = k_t^k (\Omega^k - \Omega_S^k) \tag{14}$$

The parameter k_t^k is the braking coefficient of the eddy current brake and Ω_S^k the angular velocity of the sleeve at lumped element k. The braking force is with this dependent on the relative angular velocity between the pipe and the sleeve. To achieve the most effective braking, it is desirable to keep the sleeve non-rotating ($\Omega_S^k = 0$). The sleeve slips and starts rotating when the braking force acting on the pipe is stronger than the static friction force between the borehole and the sleeve. In such a case the movement of the sleeve is defined by

$$\dot{\Omega}_S^k = \frac{1}{I_S}(r_{Si} k_t^k (\Omega^k - \Omega_S^k) - r_{So} \mathcal{F}_y^k)\,. \tag{15}$$

With Eqs. (14) and (15), the torsional dynamics of the pipe in Eq. (6) become

$$\dot{\Omega}^k I^k = \tau_-^k - \tau_+^{k+1} - r_o^k F_S^k \tag{16}$$

for $k \in S$.

For the active sleeve, the damping coefficient can be changed by moving the magnet array relative to the conductive metal. In the simulation study that follows, the controller is assumed to directly affect the braking coefficient, k_t, and not the position of the magnet array, which would be the case in practice. To account for actuator dynamics due to the magnet's inertia, the control input is low-pass filtered. That is

$$\dot{k}_t^k = \frac{1}{T_{act}}(u_c^k - k_t^k), \tag{17}$$

where u_c^k is the system input from the controller and T_{act} is the time constant of the actuator system.

The drill string simulation model used in this paper has been verified against surface and downhole data from drilling operations in Aarsnes and Shor (2018), while the sleeve braking force model (Eq. (14)) has been verified against experimental results in Holsaeter et al. (2023).

3. Controllers

In this section, the controllers used, namely On–Off and Proportional–Off (P–Off) control, are presented. For the controllers, it is assumed that the sleeves cannot communicate with each other, but know the set point RPM, and have local measurements available, such as the angular velocity of the sleeve Ω_S^k and of the pipe segment Ω^k. As shown in Eq. (17), the braking coefficient of the sleeve k_t^k is manipulated by the controller output u_c^k.

3.1. On–Off controller

The simplest controller is an On–Off controller, also known as two–state or bang–bang controller. It has only two possible outputs between which it switches, hence its name. As the On state, a maximum braking coefficient is chosen, denoted as u_{On}, while the Off state, denoted u_{Off} is set to zero. The controller is given as

$$u_{o/o}^k = \begin{cases} u_{On} & \text{for } \Omega^k > \Omega_{sp} \\ u_{Off} & \text{for } \Omega^k \leq \Omega_{sp} \end{cases}. \tag{18}$$

For the control of the sleeves, the set point angular velocity Ω_{sp} is used as the switching parameter. The idea is to brake as strongly as possible when the system is overshooting, to decelerate. If the pipe is too slow, the brake is released so the braking is not working against the necessary acceleration or even worse, stopping the entire motion of the pipe. With the high braking coefficient in the on-case and potentially high relative velocities, the sleeves are more likely to slip. To reduce the effect of the slipping of the sleeves and with this a reduced relative velocity for braking, another switching condition is added to this controller:

$$u_{On-Off}^k = \begin{cases} u_{o/o}^k & \text{for } \Omega_s^k < \Omega_{thr} \\ u_{Off} & \text{for } \Omega_s^k \geq \Omega_{thr} \end{cases} \tag{19}$$

with the slipping of the sleeve being defined as it moving faster than a threshold velocity, Ω_{thr}. In the slip case, the brake is released immediately to allow the sleeve to slow down and become stationary again. The controller can be rewritten as

$$u_{On-Off}^k = \begin{cases} u_{On} & \text{for } \Omega_s^k < \Omega_{thr} \wedge \Omega^k > \Omega_{sp} \\ u_{Off} & \text{for } \Omega_s^k \geq \Omega_{thr} \vee \Omega^k \leq \Omega_{sp} \end{cases} \tag{20}$$

and replaces the general actuation u_c^k in Eq. (17). The potential disadvantage of the On–Off controller is its rapid change in actuation close to the set point velocity. This would significantly increase wear of a real actuator.

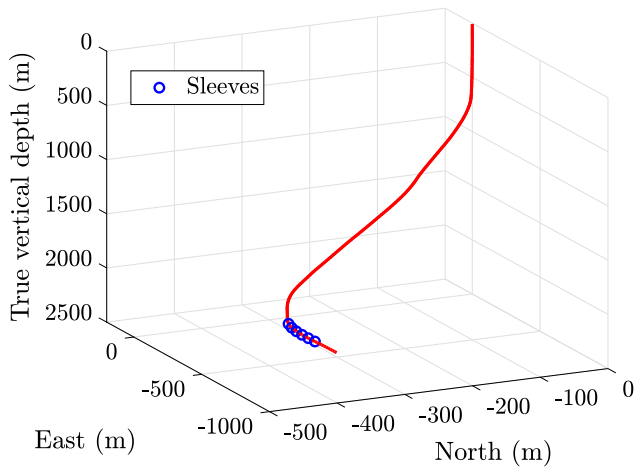

Fig. 2. Well trajectory with sleeve placement.

3.2. P–Off controller

As an improvement, a P–Off controller is designed. It consists of a P–controller with an immediate off condition. This condition is met, as before, whenever the sleeve slips or when the pipe sticks. The P–controller allows a smoother control value around the set point. The P–controller is given by

$$u_P^k = k_{P_S}(\Omega^k - \Omega_{sp}) + k_o\,, \tag{21}$$

where k_{P_S} is the proportional gain and k_o is an offset, such that there always is some braking force applied. The P–Off controller is then designed as

$$u_{P-Off}^k = \begin{cases} u_P^k & \text{for } \Omega_s^k \le \Omega_{thr} \wedge \Omega^k > \Omega_{thr} \\ u_{Off} & \text{for } \Omega_s^k > \Omega_{thr} \vee \Omega^k \le \Omega_{thr} \end{cases} \tag{22}$$

4. Simulation study

In this section, the effects of the controllers are tested for one set of drilling parameters. Here, the off-bottom case is studied, with the bit being 20 m off bottom.

4.1. Simulation setup

The simulation setup is based on the one in Ambrus et al. (2022). Both the parameters and the trajectory were chosen to represent a typical North Sea well with a long build section where the issue of stick–slip is a significant concern. Fig. 2 shows the well trajectory used. The well has a total measured depth of 2500 m and is drilled from a fixed platform with water depth of 200 m. A 0.251 m (9.875 in) casing is set at 2200 m. The reservoir section is drilled with a 0.216 m (8.5 in), 6-blade PDC bit using a rotary steerable system (RSS). The BHA is 260 m long, consisting of drill collars with an average outer diameter (OD) of 0.194 m (7.625 in). The drill string is completed with 2240 m of 0.147 m (5.78 in)-OD drill pipes with 0.168 m (6.625 in)-OD tool joints. The drilling fluid used is oil-based mud with a nominal density of 1200 kg/m^3 at 20 °C and atmospheric pressure conditions. The other physical simulation parameters are summarized in Table 1.

The drill string is simulated using 250 lumped elements. Whenever sleeves are used, six of them are placed as in Fig. 2, with 30 m distance between each other, positioned at indices $S = [225, 228, 231, 234, 237, 240]$. The sleeves have an OD of 0.191 m ($7\frac{1}{2}$ in) compared to the tool joint OD of 0.168 m ($6\frac{5}{8}$ in) to lift up the pipe. All sleeves either share the same passive braking coefficient or have the same control law

Table 1
Simulation parameters.

Parameter	Value	Unit
Drill bit diameter	0.216	m
BHA average outer diameter	0.194	m
BHA average inner diameter	0.096	m
Drill pipe tool joint diameter	0.168	m
Drill pipe outer diameter	0.147	m
Drill pipe inner diameter	0.123	m
Sleeve inner diameter	0.165	m
Sleeve outer diameter	0.191	m
Axial structural damping coefficient	217	N s/m
Torsional structural damping coefficient	0.447	N m s/rad
Drilling fluid density	1200	kg/m^3
Drill pipe density	7850	kg/m^3
Elastic modulus	200	GPa
Shear modulus	67	GPa
Top drive moment of inertia	2900	kg m^2
Static friction coefficient	0.75	
Kinetic friction coefficient	0.3	
Velocity threshold for static to kinetic friction transition	0.05	m/s
Actuator time constant	0.6	s
Number of drill bit blades	6	
Bit–rock model parameter ε	50	MPa
Bit–rock model parameter ζ	0.5	
Bit–rock model parameter γ	1	
Bit–rock model parameter μ	0.6	
Bit–rock model parameter w_f^*	60	kN/m

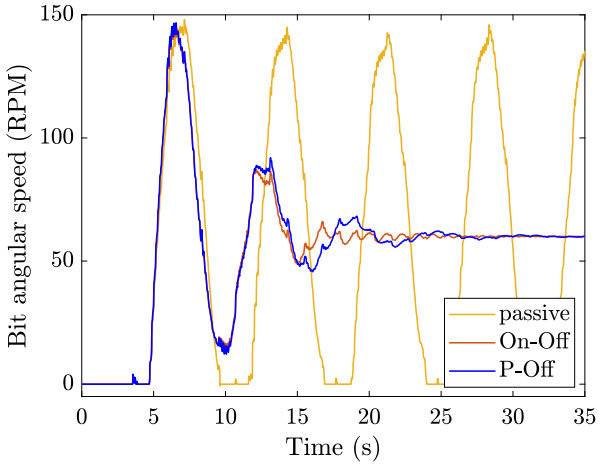

Fig. 3. Bit RPM for passive and active cases.

implemented, evaluated separately for every sleeve. The drilling scenario is chosen such that the passive sleeve, with a constant braking coefficient of 600 N s/rad, results in a stick–slip cycle and sleeves start slipping at certain points, this is used as the benchmark system and depicted in yellow in Fig. 3. To emphasize the abilities of the active sleeves, compared to the simulation parameters in Ambrus et al. (2022), the static friction was increased to 0.75, such that occurring stick–slip cycles get more severe. Feed rate and top drive RPM are set to 60 m/h and 60 RPM respectively.

For the passive case, all sleeves are slipping when there is a peak in the bit RPM. This can be seen in Fig. 4. The sleeve that is located the highest up in the drill string has the highest slip velocity resulting in a lower braking force.

4.2. On–Off controller

For the On–Off controller, the On value was set to the passive damping value of 600 N s/rad. The resulting bit RPM can be seen in

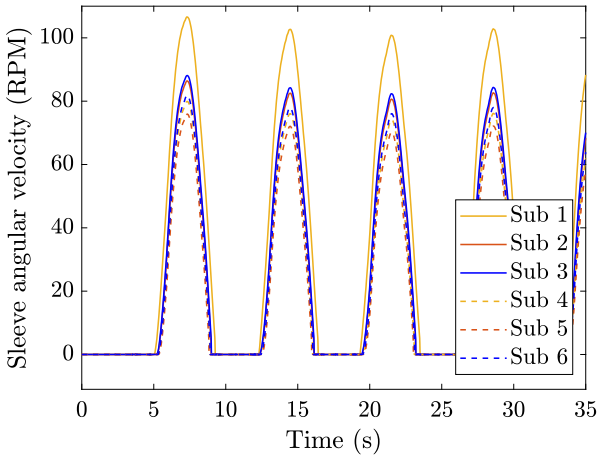

Fig. 4. Slipping of the sleeves for passive case.

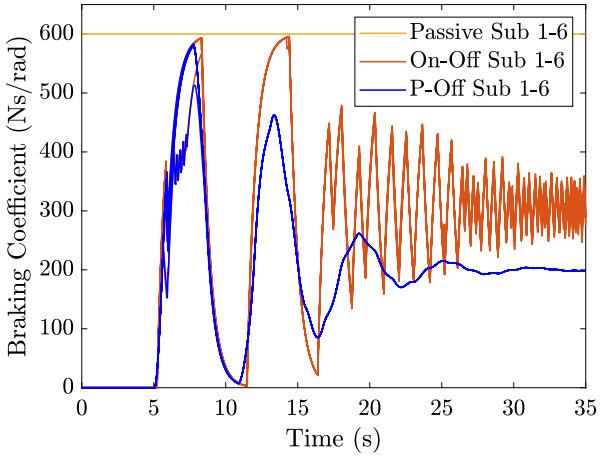

Fig. 5. Braking coefficient for passive and active cases.

Fig. 3 in red. The controller is able to mitigate the stick–slip effects and the drill bit reaches a steady state around the set point (60 RPM). Having a look at the braking coefficient after the low-pass filter (see Fig. 5, red line) reveals the disadvantage of the bang bang controller. Even though the steady state is reached, high-frequency oscillations in the actuation can be noticed.

4.3. P–Off controller

For the P–Off controller defined in Eqs. (21) and (22), all sleeves share the same controller parameters

$$k_{P_S} = 190\,\mathrm{N\,s^2/rad^2}$$
$$k_o = 200\,\mathrm{N\,s/rad}$$

Using the P–Off controller, the stick–slip cycle can be broken and a more or less constant RPM is reached (see blue line in Fig. 3).

Now, if we have a look at the control value in Fig. 5, we see that the average active braking coefficient is lowered by a third and smoothed compared to the On–Off controller. In the end, the steady state value of k_o is reached. In Fig. 6 the sleeve angular velocities are shown. Compared with the passive case in Fig. 4, the sleeves only slip within a time frame of 3 s. Also the maximum sleeve velocity is lowered to below 2 RPM, while it was above 100 RPM in the passive case.

Since the P–Off controller reaches the steady state with smoother actuator changes than the On–Off controller, it is used as an example of active control in the remaining work.

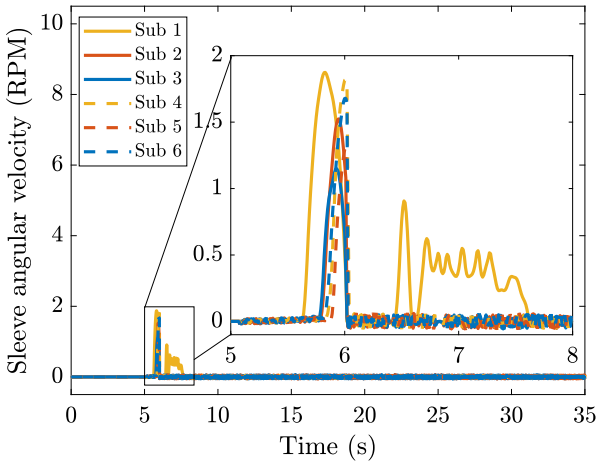

Fig. 6. Slipping of the sleeves for active case with P–Off controller.

5. Stability maps

To investigate how the controller performs for different drilling conditions, namely top drive RPM and feed rate, stability maps are used. These show whether or not the system gets stuck in a stick–slip cycle. This section builds on Aarsnes and van de Wouw (2019) and the metrics given in section 6.2 there. The idea is to check for which combination of top drive velocity V_0 and top drive RPM Ω_0 stick–slip occurs. The metric is defined by

$$M_T = \frac{\Omega_0 - \min_{t\in[T_{min},\,T_{max}]} \Omega_B(t)}{\Omega_0} \tag{23}$$

The minimum angular bit velocity Ω_B will be zero in the interval $[T_{min}, T_{max}]$ if stick occurs, and $M_T = 1$. But if the bit angular velocity stays perfectly at the top drive RPM Ω_0 during the interval $[T_{min}, T_{max}]$, then the minimum is Ω_0 and $M_T = 0$ (no downhole motors are used in this study). This is the case in the steady state. Intermediate values of M_T between 0 and 1 indicate some oscillations around the set point, but not complete sticking.

For the simulation, the same deviated well as in Section 4 is used. The performance is tested for both the bit on-bottom and off-bottom cases. In the off-bottom case, the vibrations solely come from the contact between the pipe and borehole wall, while the bit-rock interaction is the main cause of stick–slip in the on-bottom case. For comparison, several scenarios are simulated:

1. the benchmark case without sleeves
2. passive sleeves without torsional damping ($k_t = 0\,\mathrm{N\,s/rad}$)
3. passive sleeves with moderate torsional damping ($k_t = 200\,\mathrm{N\,s/rad}$)
4. passive sleeves with high torsional damping ($k_t = 600\,\mathrm{N\,s/rad}$)
5. active sleeves with P–Off controller

A uniformly spaced grid of 30 × 30 combinations of set point RPM and feed rate is used to generate the stability maps. The system is simulated for 250 s. The time interval for t has to be chosen larger than the period of a stick–slip cycle. In the simulation case presented in Section 4, the period of one stick–slip cycle was about 7 s, as can be seen from the bit RPM for the passive example (Fig. 3), so the last 20 s of every run were chosen for evaluating M_T. That is, the minimum in Eq. (23) is taken over $t \in [230, 250]$ to eliminate the effect of transients in the beginning.

5.1. Off-bottom

In Figs. 7 to 9 the stability maps for the off-bottom case are shown. The color bar indicates the value of the metric M_T, where yellow

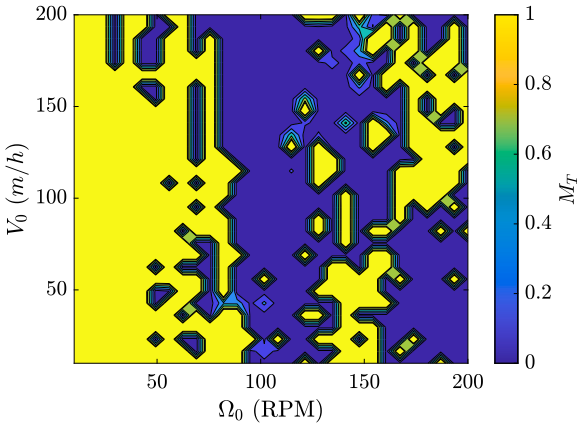

Fig. 7. Stability map for off-bottom case without sleeves.

represents stick–slip and dark blue stable conditions. For the case without sleeves in Fig. 7 a large area in the low RPM range is prone to stick–slip. With higher RPM the map gets more scattered. The scattered areas can be explained by the non-linearity of the coupled axial and torsional drill-string dynamics where a small change in the operating parameters can initiate or cure a stick–slip cycle even at high RPM set points. This is in line with previous studies (Aarsnes and van de Wouw, 2019)

Adding passive sleeves to the system, as in Fig. 8 can improve the behavior. For the case without any torsional damping in Fig. 8(a) ($k_t = 0$) the results look similar to the case without sleeves shown in Fig. 7. However, the tendency of the system to enter stick–slip oscillations is reduced even without the torsional damping since the friction is reduced as sleeves without torsional damping are equivalent to non-rotating drill pipe protectors as presented in Moore et al. (1996). As there is no torsional braking force applied in the sleeves, occurring vibrations will not be reduced, just as in the no-sleeve case. But through lifting the pipe from the borehole wall, the mechanical friction on the pipe is reduced, which reduces the source of stick–slip and the top drive torque. The torque reduction is small, as there are only 6 sleeves that are placed quite close to each other, so in most parts of the well, the drill string is still in contact with the borehole. Using a larger number of sleeves distributed along all of the drill string would lead to a more significant torque reduction, see Cayeux and Ambrus (2023).

The results in Fig. 8(b) present the case with some torsional damping. As a braking force is applied in this case, the vibrations can be reduced. The scattered characteristics are removed and the area with stick–slip decreases. Only the area of low RPM still leads to stick–slip cycles.

Increasing the damping further reduces this area (see Fig. 8(c)). A large area of the stability map is now showing that the bit RPM reaches a steady state around the set point within the simulation time. But comparing the results with the ones presented in Section 4, it is noticeable that the combination of 60 RPM and feed rate of 60 m/h seem to lead to a stable steady state in the stability map while showing a stick–slip cycle before. The stick–slip cycle is broken at some time $t > 35$ s. This shows a drawback of the metric M_T in the sense that it measures whether or not stick–slip persists beyond some initial time interval, and not how quickly stick–slip is attenuated in the stable case.

Allowing active control of the sleeves (see Fig. 9) does not lead to any further significant improvement in terms of M_T compared to the passive sleeves with high torsional damping. However, the braking torque in the steady state is lower since the steady state braking coefficient is lower, reducing the energy consumed by the top drive and reducing the wear from excessive torque on the drill string, which can be a key limitation to drilling long lateral wells. The active sleeve and the passive one with moderate damping share the same steady-state

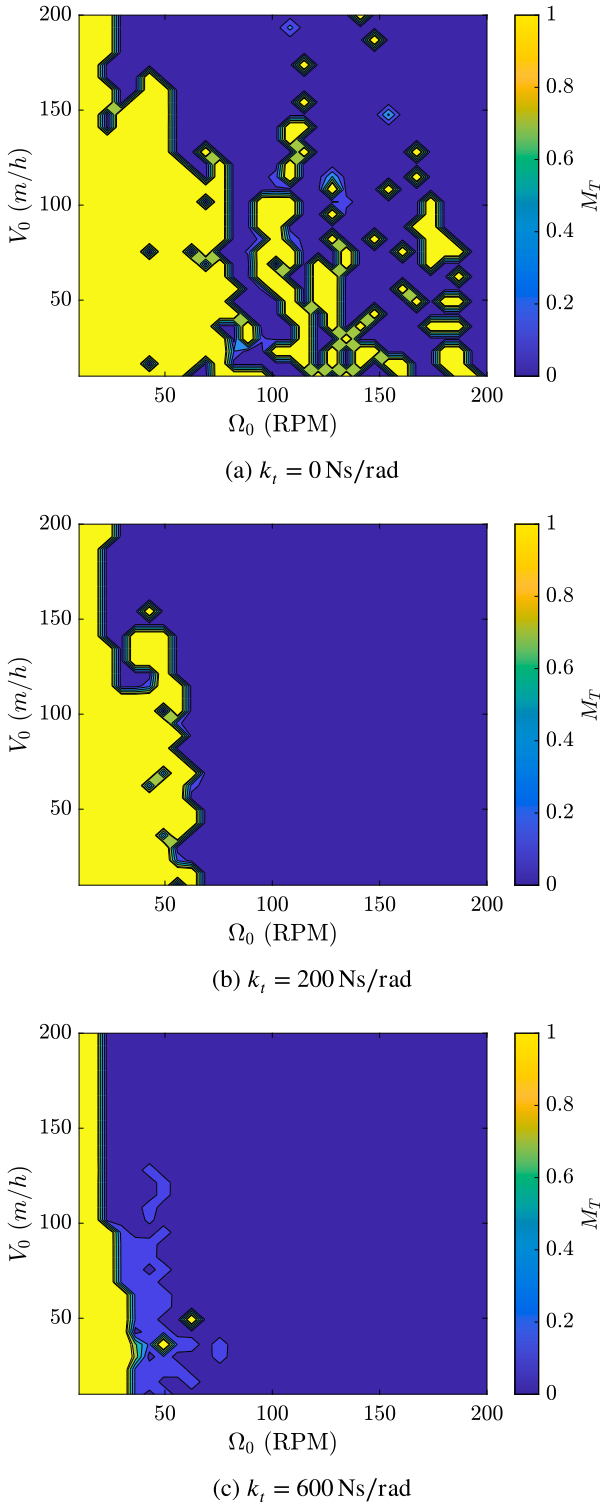

Fig. 8. Stability maps for off-bottom case with passive sleeves.

braking coefficient, which results in similar braking torques. Comparing Figs. 9 to 8(b), it is clear that active control performs better in terms of M_T than the passive case for similar top drive energy consumption.

To allow a more detailed comparison between the active sleeve and the passive one with high damping, a map based on the settling time (see Fig. 10) is used, using the point of time at which the bit angular velocity enters the 5% error band around the set point and stays within it. Disregarding the points at which the settling time is longer than

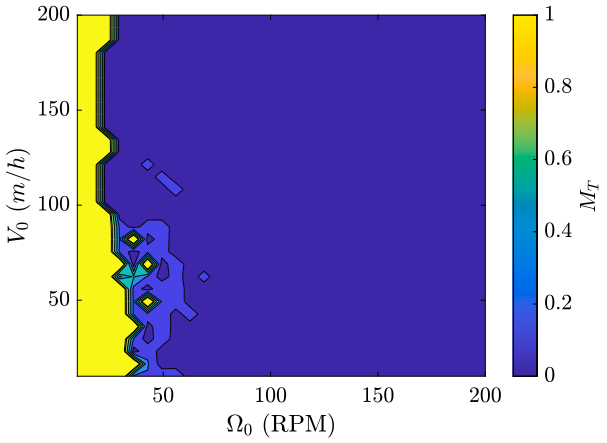

Fig. 9. Stability map for off-bottom case with active sleeves.

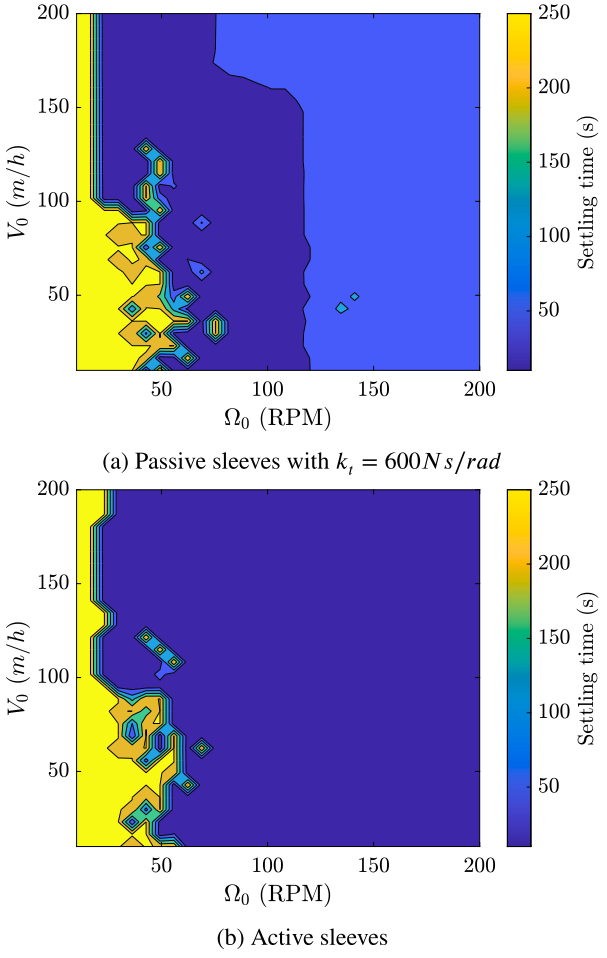

(a) Passive sleeves with $k_t = 600 N s/rad$

(b) Active sleeves

Fig. 10. Settling time (s) for off-bottom case.

250 s, the passive sleeves in Fig. 10(a) reach a settling time of up to 90 s for higher RPM, while the active sleeves system in Fig. 10(b) enters the error band within less than 30 s.

Alternating active sleeves and passive sleeves with a damping coefficient of 600 N s/rad performs as good as using only active sleeves. This could reduce the costs of the setup as passive sleeves will be cheaper to manufacture since they do not require additional sensors and electronic components that would be necessary to implement the P–Off controller described in Section 3.2. Nevertheless, the passive sleeves cannot react

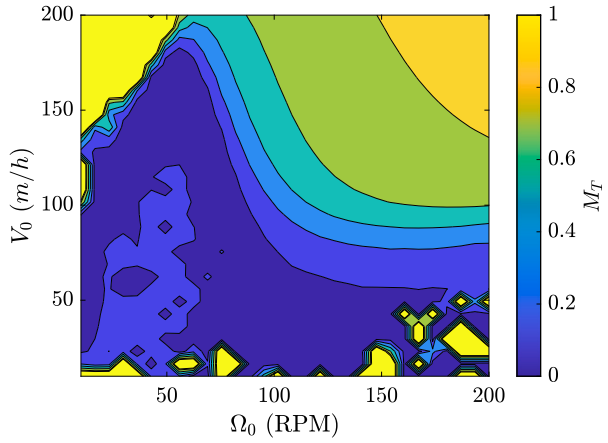

Fig. 11. Stability map for on-bottom case without sleeves.

to changes in the local friction or angular velocity, and are more likely to slip and therefore cause damage to the borehole (Cayeux and Ambrus, 2023).

5.2. On-bottom

In Figs. 11 to 13 the stability maps for the on-bottom case are presented. For the no-sleeve case in Fig. 11, several effects can be identified: For low RPM and high feed rate a clear area of stick–slip can be seen. For low feed rates, the results are scattered. For high RPM and high feed rate, oscillations can be detected. With increasing RPM/feed rate the magnitude of those oscillations increases. In the low RPM, low–moderate feed rate range, small oscillations can occur.

Adding passive sleeves, as in Fig. 12, again can improve the results. For sleeves without torsional damping (Fig. 12(a)), the results look similar to the ones without sleeves, except that the scattered area is reduced. As in the off-bottom case, the effect is small, as only a slight reduction of the mechanical friction is achieved. Using some torsional damping (Fig. 12(b)) removes the scattered parts as in the off-bottom case. Also, the severity of the oscillations in the high RPM — high feed rate area decreases significantly, while the stick–slip area in the upper left corner stays around the same. Increasing the damping (Fig. 12(c)), in contrast to the off-bottom case, does not further increase the positive effects. Here the oscillations in the high RPM — high feed rate area become greater in magnitude again as the sleeves tend to slip and therefore only apply reduced braking force.

Introducing active sleeves (see Fig. 13) removes those oscillations, as the controller is designed to reduce the slipping of the sleeve. So, a higher effective damping force can be maintained in situations in which the passive sleeves would slip. Nevertheless, the stick–slip in the upper left corner remains as before, also the area of small oscillations is present as in all scenarios. Here, the active sleeve outperforms the passive cases for all damping coefficients investigated in terms of M_T mainly in the high RPM — high feed rate area. The steady-state braking torque is comparable with the passive sleeve case with moderate damping, as in the off-bottom case.

A comparison of the settling times of the active sleeve and the passive sleeve case, here for the moderate damping case, is shown in Fig. 14. Again, disregarding the areas in which the error band is not reached at all, the passive sleeve case in Fig. 14(a) needs more than 40 s in most of the remaining area. The active sleeve case (see Fig. 14(b)) instead reaches the error band within less than 20 s in the largest remaining area.

To test a combination of active and passive sleeves, passive sleeves with a damping coefficient of 200 N s/rad are used this time, as the

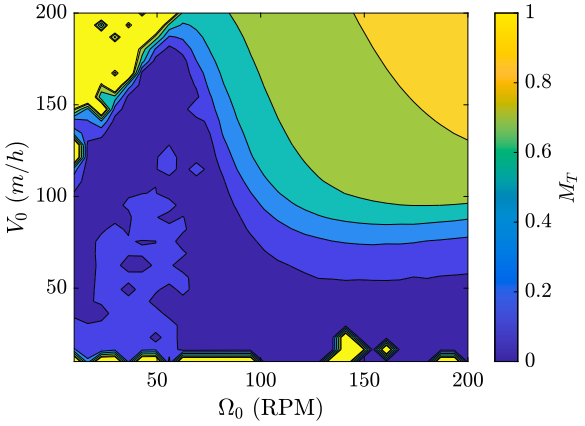

(a) $k_t = 0\,\mathrm{Ns/rad}$

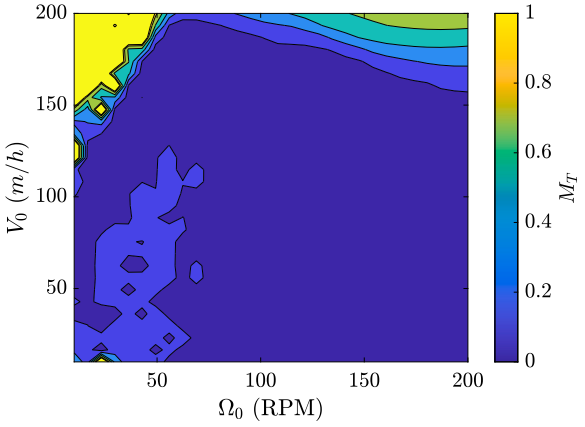

(b) $k_t = 200\,\mathrm{Ns/rad}$

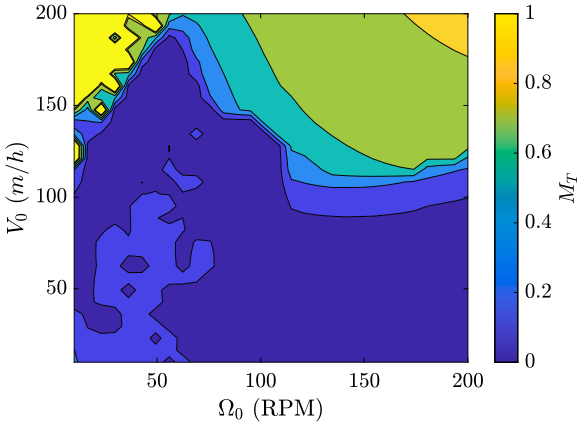

(c) $k_t = 600\,\mathrm{Ns/rad}$

Fig. 12. Stability maps for on-bottom case with passive sleeves.

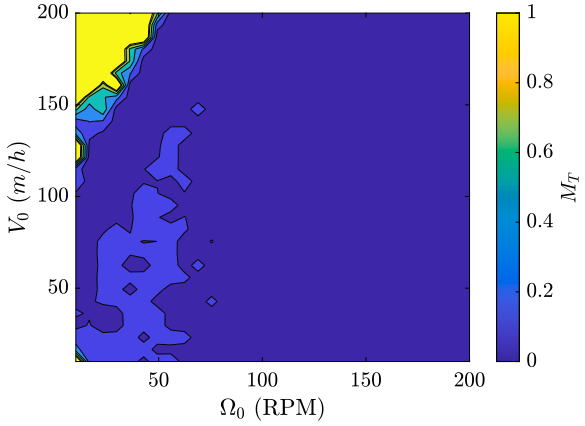

Fig. 13. Stability map for on-bottom case with active sleeves.

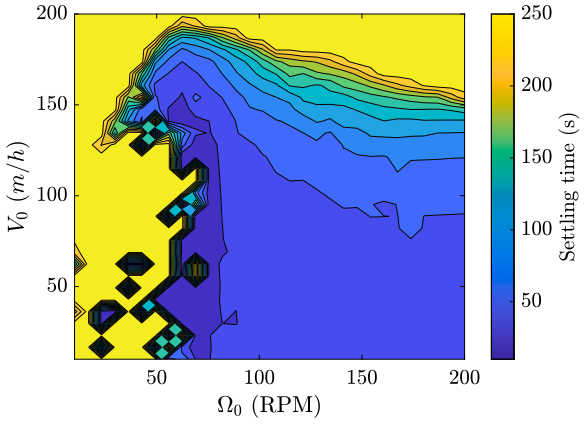

(a) Passive sleeves with $k_t = 200 Ns/rad$

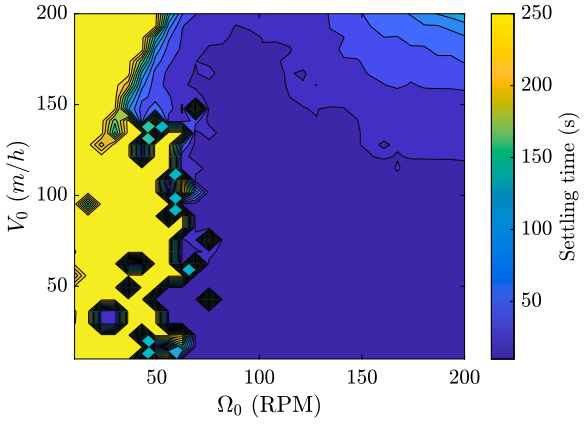

(b) Active sleeves

Fig. 14. Settling time (s) for on-bottom case.

moderate damping performed best out of the passive sleeves for the on-bottom case. The mixed sleeves perform slightly worse than the active sleeves, as they cannot fully mitigate oscillations for very high feed rates and RPM set points.

Removing the stick–slip also ensures a more stable depth of cut and bit axial velocity during the drilling operation, which can facilitate improved drilling performance and borehole quality (Ambrus et al., 2022). On the other hand, when the pipe is moving axially (i.e., during drilling or reaming operations), the friction in the axial direction would be higher with the active sleeves since the P–off controller effectively prevents rotation of the sleeves that would offset the axial friction. This may lead to increased risk of axial sticking at the sleeve locations and reduced weight transfer to the bit. However, the damping sub design investigated in our paper includes spur wheels mounted on the outside

of the sleeve which reduce the axial friction, and therefore reduce the risk of pipe sticking and also improve the weight transfer to the bit (Cayeux and Ambrus, 2023).

6. Conclusion

Drill string vibrations are a significant problem in drilling. One effective approach to mitigate torsional vibrations is using distributed damping sleeves. By incorporating eddy current brakes, viscous damping can be introduced to the system. While the sleeves are designed to remain stationary, under certain conditions they can slip, resulting in decreased braking force. Active control can be employed to improve the vibration mitigation behavior of the system. In this paper, a P–Off controller was presented for this purpose. To allow a performance comparison between a drill string with active, passive, or without sleeves, stick–slip-based stability maps were used. The simulations demonstrate the superiority of active control over passive sleeves with a fixed braking coefficient when using only a few sleeves. The results indicate that the controller can remove stick–slip for most realistic operating conditions. More precisely, in the presented on-bottom case the active controller is able to remove the vibration area from around 100 RPM and higher and feed rates of 75 m/h and above. The stick–slip area for feed rates below 50 m/h is removed while the one for angular velocities below 50 RPM and feed rates higher than 150 m/h remains unchanged. Moreover, the torque input can be reduced compared to passive sleeve configurations that produce similar stability maps. By reacting to possible sleeve slippage, settling times can be shortened by two to three times relative to passive sleeves with comparable braking coefficients. Overall, the findings of this study demonstrate the potential for active control to improve the vibration mitigation performance of the sleeves.

Declaration of competing interest

The authors declare that they have no known competing financial interests or personal relationships that could have appeared to influence the work reported in this paper.

Data availability

No data was used for the research described in the article.

Acknowledgments

This work is part of the Center for Research-based Innovation DigiWells: Digital Well Center for Value Creation, Competitiveness and Minimum Environmental Footprint (NFR SFI project no. 309589, https://DigiWells.no). The center is a cooperation of NORCE Norwegian Research Centre, the University of Stavanger, the Norwegian University of Science and Technology (NTNU), and the University of Bergen. It is funded by Aker BP, ConocoPhillips, Equinor, Lundin Energy, TotalEnergies, Vår Energi, Wintershall Dea, and the Research Council of Norway.

References

Aarsnes, U.J.F., Di Meglio, F., Shor, R.J., 2018. Avoiding stick slip vibrations in drilling through startup trajectory design. J. Process Control 70, 24–35. http://dx.doi.org/10.1016/j.jprocont.2018.07.019, URL: https://www.sciencedirect.com/science/article/pii/S0959152418301859.

Aarsnes, U.J., Di Meglio, F., Shor, R., 2018. Benchmarking of industrial stick-slip mitigation controllers. IFAC-PapersOnLine 51, 233–238. http://dx.doi.org/10.1016/j.ifacol.2018.06.382.

Aarsnes, U.J.F., Shor, R.J., 2018. Torsional vibrations with bit off bottom: Modeling, characterization and field data validation. J. Pet. Sci. Eng. 163, 712–721. http://dx.doi.org/10.1016/j.petrol.2017.11.024, URL: https://www.sciencedirect.com/science/article/pii/S0920410517309075.

Aarsnes, U.J.F., van de Wouw, N., 2019. Axial and torsional self-excited vibrations of a distributed drill-string. J. Sound Vib. 444, 127–151. http://dx.doi.org/10.1016/j.jsv.2018.12.028, URL: https://www.sciencedirect.com/science/article/pii/S0022460X1830854X.

Ambrus, A., Aarsnes, U.J.F., Cayeux, E., Mihai, R., 2022. Modeling and analysis of non-rotating damping subs for removing torsional vibrations in drilling. In: International Conference on Offshore Mechanics and Arctic Engineering, Volume 10: Petroleum Technology. http://dx.doi.org/10.1115/OMAE2022-78339, V010T11A084.

Azike-Akubue, V., Barton, S., Gee, R., Burnett, T., 2012. Agitation tools enables significant reduction in mechanical specific energy. In: SPE Asia Pacific Oil and Gas Conference and Exhibition. All Days, http://dx.doi.org/10.2118/158240-MS, SPE-158240-MS.

Barton, S., Baez, F., Alali, A., 2011. Drilling performance improvements in gas shale plays using a novel drilling agitator device. In: SPE Unconventional Resources Conference / Gas Technology Symposium, Vol. All Days. http://dx.doi.org/10.2118/144416-MS, SPE-144416-MS.

Cayeux, E., Ambrus, A., 2023. Self-attenuation of drillstring torsional vibrations using distributed dampers. SPE J. 1–22. http://dx.doi.org/10.2118/214675-PA.

Detournay, E., Richard, T., Shepherd, M., 2008. Drilling response of drag bits: Theory and experiment. Int. J. Rock Mech. Min. Sci. 45 (8), 1347–1360. http://dx.doi.org/10.1016/j.ijrmms.2008.01.010, URL: https://www.sciencedirect.com/science/article/pii/S1365160908000245.

Dong, G., Chen, P., 2016. A review of the evaluation, control, and application technologies for drill string vibrations and shocks in oil and gas well. Shock Vib. 2016, 7418635. http://dx.doi.org/10.1155/2016/7418635.

Dwars, S., 2015. Recent Advances in Soft Torque Rotary Systems. In: SPE/IADC Drilling Conference and Exhibition, Vol. Day 3 Thu, March 19, 2015. http://dx.doi.org/10.2118/173037-MS, D031S016R006.

Feng, T., Zhang, H., Chen, D., 2017. Dynamic programming based controllers to suppress stick-slip in a drilling system. In: 2017 American Control Conference. ACC, pp. 1302–1307. http://dx.doi.org/10.23919/ACC.2017.7963132.

Ghasemloonia, A., Geoff Rideout, D., Butt, S.D., 2015. A review of drillstring vibration modeling and suppression methods. J. Pet. Sci. Eng. 131, 150–164. http://dx.doi.org/10.1016/j.petrol.2015.04.030, URL: https://www.sciencedirect.com/science/article/pii/S0920410515001795.

Holsaeter, A., Ambrus, A., Cayeux, E., Mihai, R., Moi, S., 2023. Experimental verification of vibration mitigation through a viscous damping system along the drill string. In: SPE/IADC Drilling Conference and Exhibition, Vol. Day 1 Tue, March 07, 2023. http://dx.doi.org/10.2118/212521-MS, D011S001R003.

Hutchinson, M., 2013. Automated downhole vibration damping. In: SPE/IADC Middle East Drilling Technology Conference and Exhibition, Vol. All Days. http://dx.doi.org/10.2118/166736-MS, SPE-166736-MS.

Kulke, V., Ostermeyer, G.-P., Hohl, A., 2021. Design and investigation of a nonlinear damper based on energy dissipation through shock and dry friction to suppress critical self-excited vibrations in drilling systems. Shock Vib. 2021, 5089213. http://dx.doi.org/10.1155/2021/5089213.

Moore, N., Mock, P., Krueger, R., 1996. Reduction of drill string torque and casing wear in extended reach wells using non-rotating drill pipe protectors. In: SPE Western Regional Meeting, Vol. All Days. http://dx.doi.org/10.2118/35666-MS, SPE-35666-MS.

Wildemans, R., Aribowo, A., Detournay, E., Wouw, N., 2019. Modelling and dynamic analysis of an anti-stall tool in a drilling system including spatial friction. Nonlinear Dynam. 98, http://dx.doi.org/10.1007/s11071-019-05075-6.

Wilson, J.K., Heisig, G., Freyer, C., 2022. HFTO Solved: Proven Mitigation of High Frequency Torsional Oscillations in Motor-Assisted Rotary Steerable Applications. In: SPE/IADC Drilling Conference and Exhibition, Vol. Day 1 Tue, March 08, 2022. http://dx.doi.org/10.2118/208739-MS, D011S003R001.

Zhao, J., 2020. Development status and application prospect of semi-active vibration reduction technology for down-hole drilling tools. IOP Conf. Ser. Earth Environ. Sci. 514 (2), 022013. http://dx.doi.org/10.1088/1755-1315/514/2/022013.